Journal of Hydraulic Structures
J. Hydraul. Struct., 2023; 9(3):32-51
DOI: 10.22055/jhs.2023.45326.1274

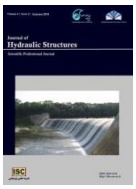

OPEN ACCESS

Experimental study of Bed Pattern around the Cylindrical Pile under Broken Waves

Akbar Kiasalary [1]
Ahmad Reza Mostafa Gharabaghi [2]

Abstract

Cylindrical piles are often used in most of coastal and offshore structures such as bridges, wharfs, offshore wind turbine foundations and Oil platforms. Most of these structures are installed in shallow water and exposed to strong currents, waves and broken waves. These phenomena can cause scour around them which can damage their structural integrity and stability. In literature, scour process around the cylindrical piles under currents and waves have been studies frequently. However, there are very little knowledge about the bed forms due to the broken waves. In this paper, the effect of broken waves on the characteristics of bed forms around a cylindrical pile has been studied experimentally in a large wave flume. The three-dimensional bed topography was measured by Close Range Photogrammetry. Vortex ripples and truncated cone scour with vortex ripples were the main observed scour pattern. Shields parameter as well as Keulegan-Carpenter (KC) number were used as the non-dimensional parameters for bed form classification. It is noticed that the ripple height and ripple steepness for broken regular waves is less than non-breaking regular waves. However, the relative equilibrium scour depth for broken waves is larger than non-breaking waves.

Keywords: Cylindrical Pile; Broken Waves; Bed Pattern; Vortex Ripple; Truncated Cone Scour.

Received: 20 November 2023; Accepted: 06 December 2023

1. Introduction

The flow regime around a vertical circular cylinder is a complex process in the classical hydrodynamics. The presence of the cylinder causes several changes in the fluid flow as shown in Fig. 1. For slender pile which the ratio of its diameter (D) to the wavelength (L_w) is less than 0.2, it blocks the fluid so the flow velocity decreases to zero on the upstream face of cylinder producing an increased pressure on that side and a significant pressure gradient that opposes the flow direction generating a down flow. This can create a scour hole in erodible beds. Consequently, the flow boundary layers close to the bed will separate along the bed in three dimensions leading to the horseshoe vortices. Moreover, the separated boundary layers create spiral vortices near the cylinder which are carried downstream by the flow which generates lee-

[1] Faculty of Civil Engineering, Sahand University of Technology, East Azerbaijan Province, Tabriz, Iran.
[2] Faculty of Civil Engineering, Sahand University of Technology, East Azerbaijan Province, Tabriz, Iran. E-Mail:mgharabaghi@sut.ac.ir, Tel: +984133444344 **(Corresponding author)**

wake vortices. They also increase the local scour process in the erodible beds. In addition, the streamlines contract at the sides of the pile and a pair of counter-rotating vortices is formed at the lee wake further downstream of the cylinder. It should be noticed that the situation is almost similar for the waves compared to the current for slender piles. However, the importance of the horseshoe vortices relative to the lee-wake vortices can be different. It is noticed that the drag force induced by the waves on seabed can be 4 times the undisturbed situation while for the current it is 10 times larger which indicates that the horseshoe vortices are stronger for the currents [1]. In order to distinguish their importance, the non-dimensional Keulegan-Carpenter number ($KC = U_m T/D$, where T is wave period and U_m is the amplitude of wave induced bottom orbital velocity) can be used to determine the role of horseshoe and lee-wake vortices. When KC is greater than 1, flow separation occurs leading to the formation of tail vortices and when it gets greater than 6, horseshoe vortices are generated, so lee-wake vortices are more capable to transport sediment away the pile [1]. For $2.8 \leq KC < 4$, a pair of symmetrical tail eddies are appeared, while for $4 \leq KC < 6$, they become asymmetrical. Vortex shedding starts for $6 \leq KC < 17$ only on one side of the pile per half cycle of wave and it alternates when $17 \leq KC < 23$ which can spread to the rear side of the pile [2]. However, for large piles where the ratio of D / L_w is larger than 0.2, wave diffraction is the dominant process.

All of these processes will change the fluid flow features especially close to the bed adjacent to the pile. When the near bed fluid velocity and its related shear stress applied to the sediment particles becomes greater than the critical value, scouring process can be started. From geotechnical aspect, the critical velocity and its related critical shear stress which are dependent on the flow and sediment properties, are the main parameters in scour process. The erosion mechanism due to the wave action is different from the current. It is also different for cohesive and non-cohesive soils. The weight, size, gradation and shape of sediment particles in addition to the interaction between them and their other properties can affect the sediment transport mechanism. This can happen by sliding, rolling, jumping (saltation) and suspended motions. The natural bed slope and the developed bed forms due to sediment transport can also disturb this process.

Shields Parameter as a non-dimensional parameter which is the ratio of applied flow forces to the stabilized submerged particle weight, can be used as a criterion for initiation of sediment motion. Shields parameter which was defined by Shields [3], ($\Theta = (U_*)^2/((s-1)gd_{50})$, where U_* is the bed shear velocity, s is relative density, g is ground acceleration and d_{50} is median particle diameter of the bed material) when raises greater than a critical value (θ_{cr}), the particles start to move. The bed shear velocity is related to the bed shear stress ($\tau_* = \rho\ U_*^2$) and is calculated from $U_* = \sqrt{\frac{f}{2}}\breve{U}_\delta$, where $\breve{U}_\delta$ is the maximum near bed orbital velocity at the edge of the wave boundary layer and f is the friction factor which according to Jonsson [4, 5] for laminar flow that its related Reynolds number ($Re = (\breve{U}_\delta \breve{A}_\delta)/\upsilon$)< 10^4, where $\breve{A}_\delta$ is the maximum value of near bed orbital excursion at the edge of the wave boundary layer and υ is the fluid kinematic viscosity, $f = 2Re^{-0.5}$ and for smooth turbulent flow ($10^4 < Re < 10^6$ and $\breve{A}_\delta / k_s > 10^3$), where k_s is the effective bed roughness height, $f = 0.09Re^{-0.2}$. Fredsøe and Deigaard [6] suggested another relation for the friction factor as: $f = 0.035Re^{-0.16}$.

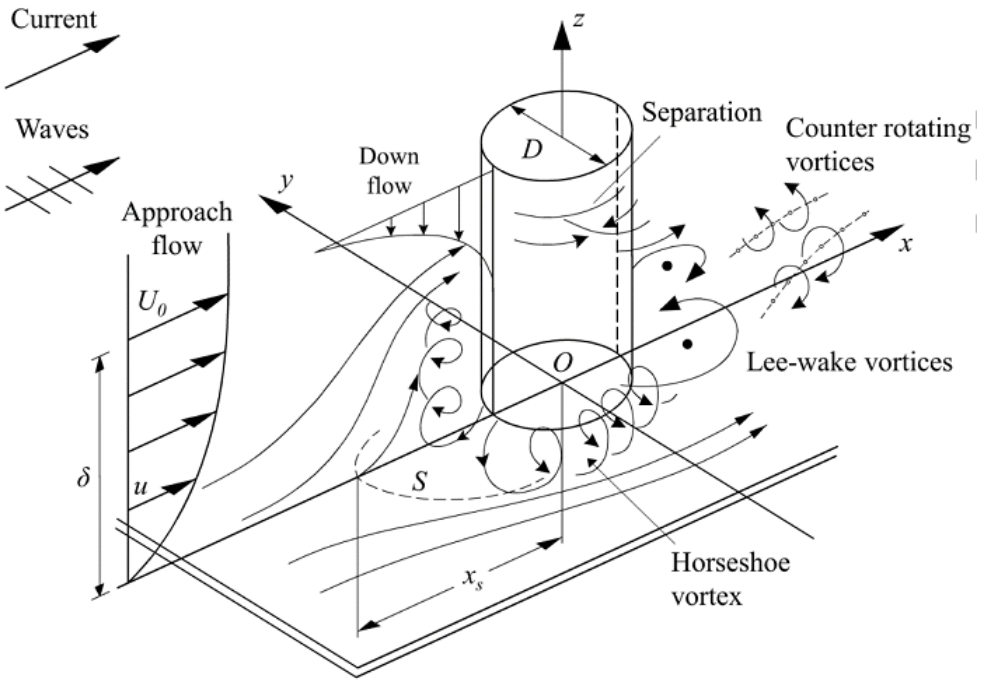

Figure 1. Flow pattern around a vertical circular cylinder (S: separation line, δ is the boundary layer thickness, x_s is the length characterizing the size of the horseshoe vortex)

Consequently, the bed forms can be developed due to the sediment motion but there are just limited studies about that. In literature, sufficient studies were made about the bed forms due to waves. Two typical regimes can be observed for wave related bed forms:

- Lower regime with flat immobile bed, ripples and bars,
- Upper regime with flat mobile bed (i.e., sheet flow)

A classification diagram is given by Allen [7] which is based on the 648 data sets. Ripples are washed out when the mobility parameter ($\Psi = \left(\breve{U}_\delta\right)^2/((s-1)gd_{50})$) is larger than about 200 to 250 (Dingler-Inman [8]; Horikawa et al. [9]). This regime is referred to as the sheet flow regime. According to Wilson [10], the sheet flow regime is present for $\Theta \geq 0.8$.

However, these regimes are changed by the presence of the pile. The mechanism of scouring around the piles under wave and or current action have been investigated in several studies. There are several comprehensive publications about it such as Chiew and Melville [11], Sumer et al. [12], Melville [13], Melville and Coleman [14], Sumer et al. [15], Sumer and Fredsoe [16], Sheppard [17], Coleman [18], Elsebaei [19], Amini Baghbadorani et al. [20], Chen and Li [21], Gazi et al. [22], Liang et al. [23], Guan et al. [24] and Li et al., 2023 [25]. Umeda [26] investigated the scour process around a pile due to the wave action by 143 experiments. He identified ten different regimes for scour patterns, mainly based on the KC number and the Shields parameter. These regimes were classified according to the shape of the scour hole and ripple pattern as: (I-1) small scour, (I-2) side scour, (I-3) wake scour, (I-4) wake and semi-cone scour, (I-5) truncated-cone scour, (II-1) detached scour, (II-2) wake scour with rolling-grain ripples, (II-3) truncated-cone scour with rolling-grain ripples, (III-1) vortex ripples, and (III-2) truncated-cone scour with vortex ripples (Fig. 2).

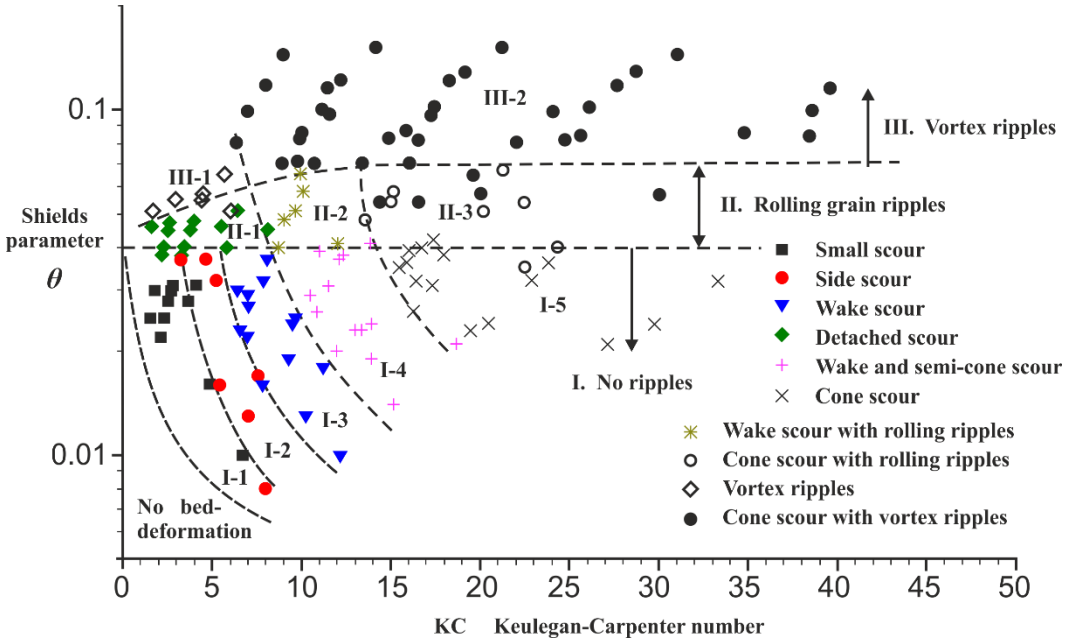

Figure 2. Classification of scour regimes for a vertical cylinder exposed to regular waves [26]

It should also be noticed that as waves propagating to the shore, they will experience breaking in the near-shore zone where some of these piles may be installed in there. Usually this is followed by wave energy dissipation, production of turbulent vortices and highly aerated and turbulent bores which can be diverted to the seabed and affect the sediment movement pattern leading to the complex bed forms [27].

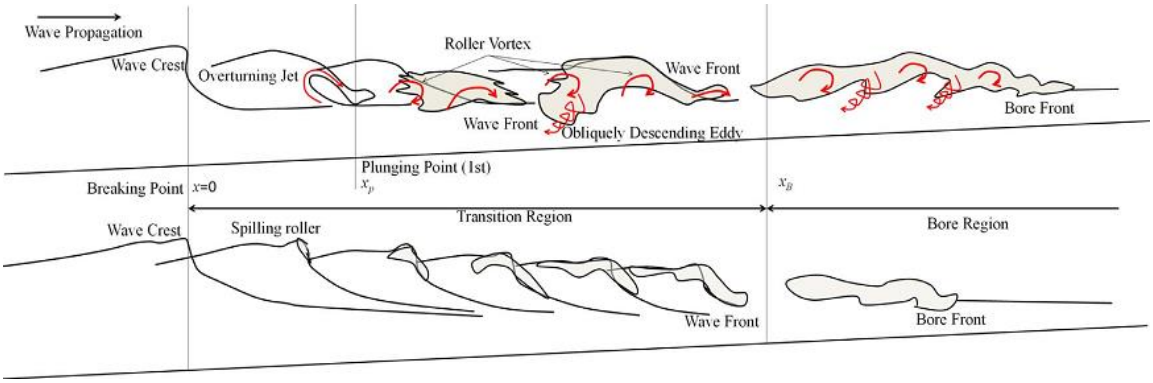

Figure 3. Schematic illustration of evolution of breaking waves; plunging (top), spilling (bottom) breaker [27]

There are a few studies about the scouring around a pile induced by breaking or broken waves which consist of full 3D fluid-structure-sediment interactions. Bijker and Bruyn [28] investigated the scouring around a pile under combined breaking waves and current. They concluded that the generated scour hole is larger than the hole related to wave-only and current-only cases. They didn't provide the results related to just wave breaking case. Later, Carreiras et al. [29] made some experiments about pile scouring due to breaking waves on a 1:20 slope. They

concluded that, “When the pile is located at the breaking point or onshore of it, global large scale bed changes, namely the formation of the bar, are superposed to the local scour processes”. Frigaard et al. [30] investigated the effect of breaking waves on scour processes around circular Offshore Wind Turbine Foundations (OWTFs). They studied the scour process in both physical and numerical models. It was a part of a more comprehensive study on scour around OWTs in areas with strong currents. They concluded that the wave breaking has only a small effect on the scour hole development. Nielsen et al. [31] experimentally studied the scour process around mono piles caused by regular breaking waves. They monitored the development of the scour depth by a camera inside the pile and used some point gauges to estimate bed morphology. They found that the maximum scour depth was approximately about 0.6 D which is smaller than current created scour however in some cases an order of magnitude larger than scour caused by non-breaking waves. Liu et al. [32] developed a 3D numerical model of non-breaking and breaking wave-induced scour around the mono pile on the Open FOAM platform.

It can be realized that there is just limited research about the scour process around a pile due to breaking or broken waves. Therefore, in this research an experimental investigation was performed to measure the bed morphology due to the broken waves around a slender vertical cylinder.

2. Experimental procedure

The experiments were carried out in a well-controlled programmable wave generating facility, located at Department of Coastal and River Engineering, Soil Conservation and Watershed Management Research Institute (SCWMRI), Iran. Its wave flume is 33 m long, 5m wide and 0.9m deep. It has a piston-type wave maker at one end which can generate both regular and irregular waves and rubble mound wave absorber at the other end as shown in Fig.4.

Figure 4. A close picture of SCWMRI’s wave flume

2.1. Experimental setup

The flume is divided into three parts: 2 side channels with two meters width and middle channel of one meter width by partition walls which are installed 4.3 m away from the wave generator. The experiments were performed in the middle channel. A sloped steel section was installed across the entire width of it, 4 m long and 35 cm height, beginning approximately 23 m from the wave paddle as shown in Fig. 5. Sediment reservoir, 2 m long, was placed after the inclined part across the entire width of the middle channel. The PVC model pile with 0.11 m diameter was installed in it, 0.8 m away from the sloped section. Flume end is made by plexiglass to view the inside of flume.

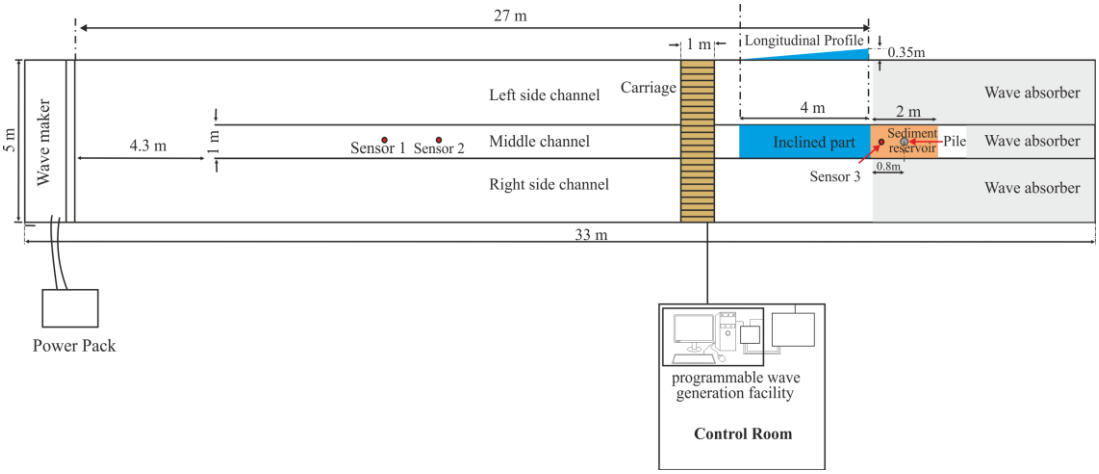

Figure 5. Plan view of the wave flume

2.2. Sediment particles preparation

Sediment reservoir was filled with selected fine sand from SCWMRI's sediment samples after sieving and clearing. The sieve analysis test is performed on the chosen sample in the laboratory. The gradation curve of sample sediments is shown in Fig. 6. The specific gravity of sediments was determined about 2.6 with d_{50}=200μm.

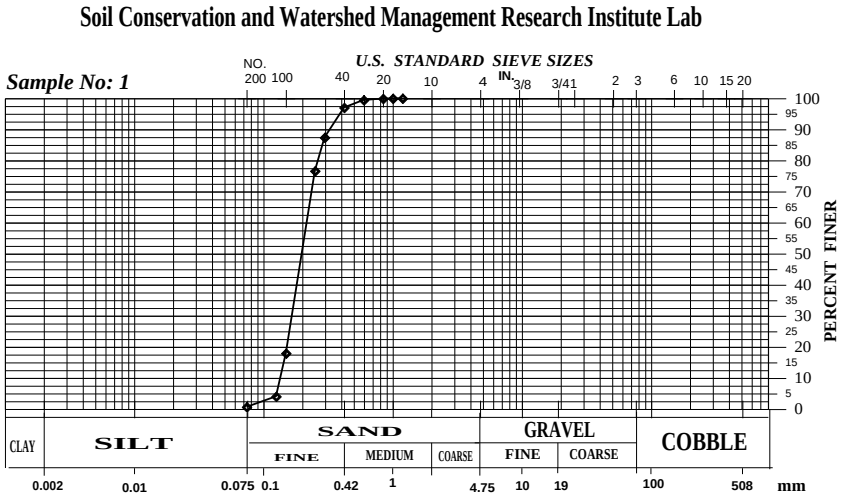

Figure 6. Gradation curve of sediment sample

2.3. Data Acquisition

In order to measure the water surface elevation, three wave gauges were installed at different sections of the wave flume, two gauges at the entrance of middle part of channel before the start of inclined part, about 0.7 meters apart each other and third one close to the wave breaking point (Fig. 5). They were calibrated before installation. The recorded elevations of gauge 1 and 2 were used to eliminate the wave reflection effects according to the proposed method by Goda and Suzuki [33]. A typical result for one of the tests is shown in Fig. 7. The position of third gauge was variable, in order to measure wave height close to the wave breaking point.

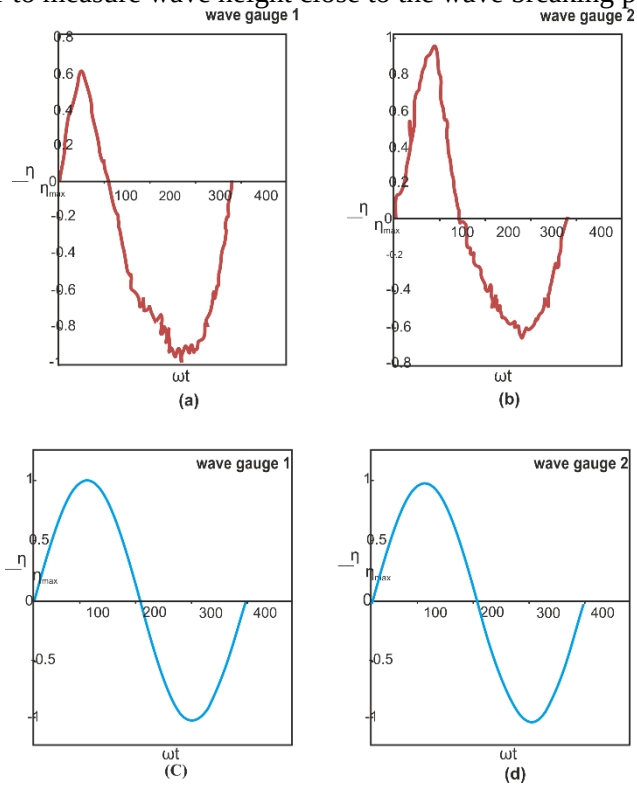

Figure 7. A typical recorded water surface elevation at gauge 1 and 2 before (a & b) and after (c & d) elimination of wave reflection effects

For mapping bed surface within a hydraulic model test, several techniques are currently available: wool threads, point gauges, echo sounders, and optical techniques. Optical techniques such as projection Moiré, photogrammetric, and 3D bed profilers allow measuring the whole bed surface instantaneously and thus experimental work can continue with lowest delays. The photogrammetric methods are the most commonly used techniques to obtain high-resolution Digital Elevation Models (DEMs) from fluvial surfaces in the laboratory and field. The capability of this method to measure surfaces in a non-intrusive way makes it a good alternative to quantify changes in the sediment beds in laboratory experiments. The digital photogrammetry was applied in this study [34]. For this purpose, a digital high-quality camera was used for imaging of the bed. Its specifications are presented in Table 1.A wooden frame and metal rail was installed over the channel walls at elevation of about 1.06 m above the bed, so the camera can move easily across and along the channel (Fig. 8).

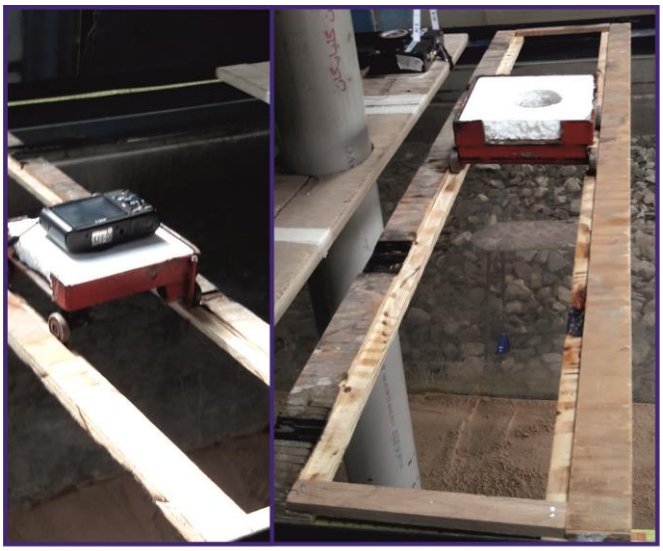

(a) (b)

Figure 8. Digital photogrammetry (a) Digital camera (b) Wooden frame and metal rail to set camera

Table 1. The specifications of Camera

Camera Model	Resolution	Focal Length	Pixel Size	Pre-calibrated
Canon Power Shot SX160 IS (5mm)	3456x3456	5 mm	1.34 x 1.34 µm	No

For accurate monitoring of the bed hydrography, vertical photos were taken at 20 points, four rows with five points in each row, in addition to another horizontal photos from 8 points for a suitable coverage of studied area as shown in Fig. 9.

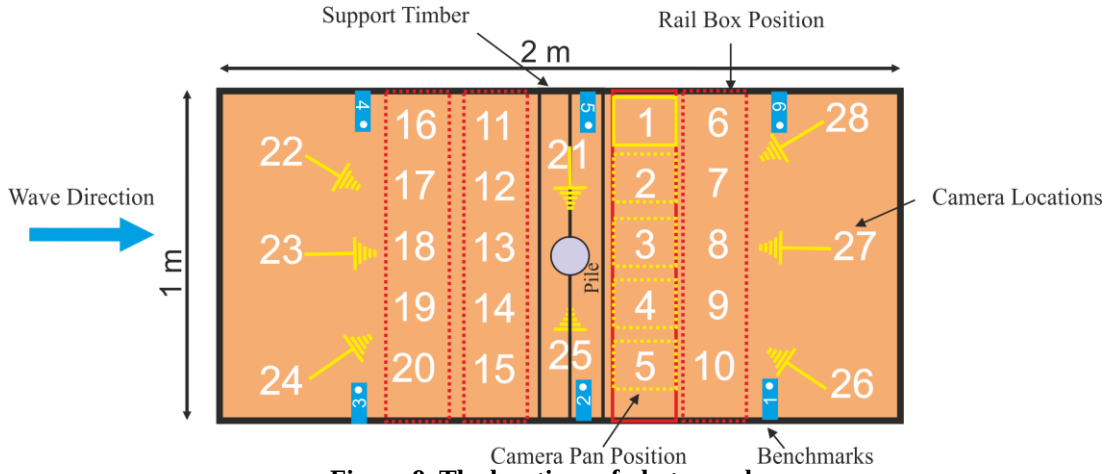

Figure 9. The locations of photography.

Moreover, in order to determine the accurate position of wave breaking point, several horizontal photos were taken from it and the photos are processed by Aoao Video to Picture Converter software. The distance between the model pile to the identified breaking point was determined by Digimizer software.

2.4. Ground Control Points (GCPs)

Six benchmarks were installed on the side walls of channel for elevation measurement (Fig. 10). Leica TS06 Plus 5" R500 Total Station was used for surveying and determining the elevation of these benchmarks.

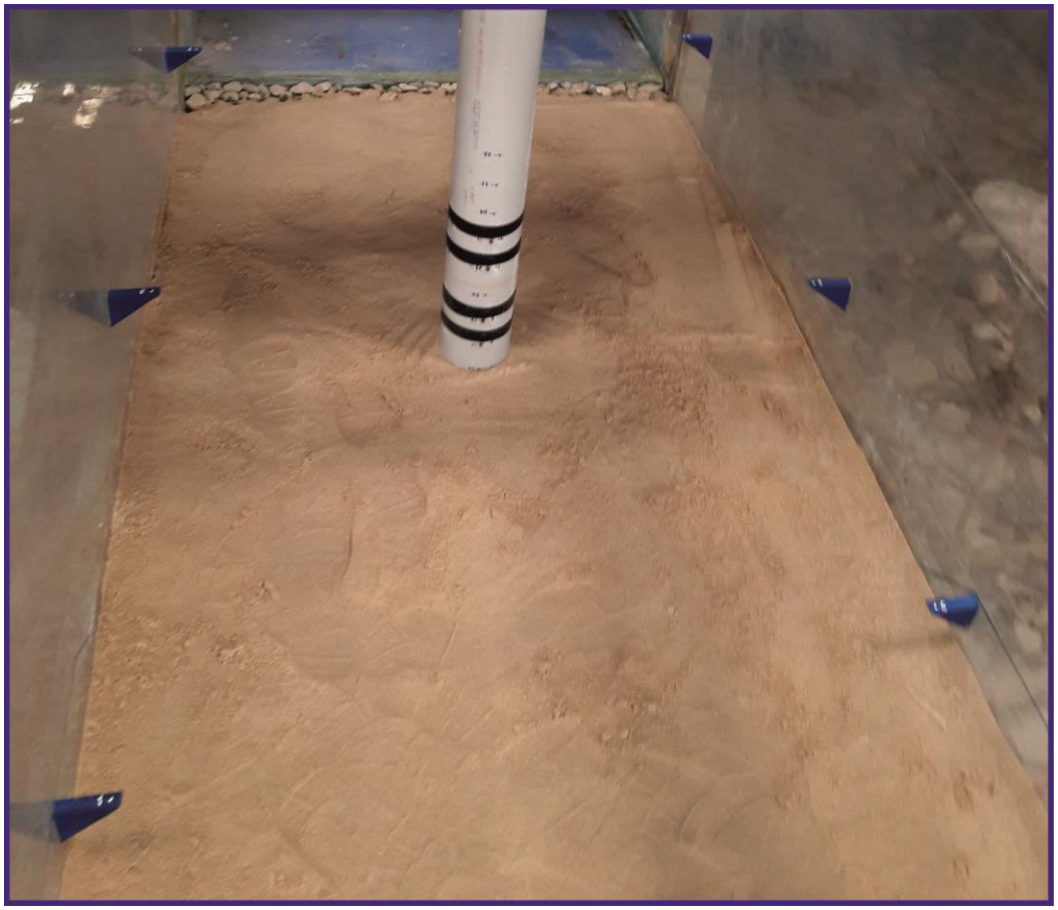

Figure 10. GCPs locations on Plexiglass wall

2.5. Wave Condition

More than 25 tests were performed and different regular waves with wave heights (H) ranging from 0.05 m to 0.15 m and wave period (T) from 1 to 2.99 seconds were generated. The characteristics of these tests are presented in Table 2. The water depth (h) varied between 0.4 m to 0.51 m. The non-dimensional parameters such as Keulegan-Carpenter number ($KC = U_m T/D$), Reynolds number ($Re = (\check{U}_\delta \check{A}_\delta)/\upsilon$) and Shields parameter ($\Theta = (U_*)^2/((s-1)gd_{50})$) are also presented in the table. The surf similarityparameter or Iribarren number ($Ir = \tan\alpha\ (H/L_0)^{-0.5}$, where, α is the slope angle and L_0 is the deep water wave length = $g\ T^2 / 2\pi$) was also calculated in order to distinguish the wave breaking type. For Spilling breaker type $0 < Ir < 0.4$, for Plunging breaker type $0.4 < Ir < 2$, and for Surging breaker type $Ir > 2$ [27]. It is noticed that the most of the breaking waves were plunging type. The wave height at the breaking point (H_b) and its position was measured by photography and wave gauge no. 3.

Table 2. Wave conditions and related parameters

Test number	h(m)	T(sec)	H(m)	H_b(m)	KC	Re	θ	Breaking Type
1	0.46	1.00	0.08	0.10	0.690	916	0.061	Spilling
2	0.41	2.04	0.05	0.06	2.108	4197	0.064	Plunging
3	0.49	2.00	0.11	0.13	4.173	16776	0.108	Plunging
4	0.45	2.54	0.13	0.15	8.371	53149	0.214	Plunging
5	0.45	2.52	0.12	0.15	7.303	40781	0.174	Plunging
6	0.44	2.99	0.09	0.09	6.630	28323	0.110	Plunging
7	0.46	2.48	0.13	0.14	7.798	47240	0.199	Plunging
8	0.46	1.47	0.08	0.09	1.708	3824	0.084	Plunging
9	0.45	2.23	0.08	0.09	3.783	12368	0.076	Plunging
10	0.45	2.41	0.09	0.11	4.734	17917	0.094	Plunging
11	0.40	2.79	0.05	0.06	3.111	6685	0.059	Plunging
12	0.46	2.40	0.08	0.10	4.279	14702	0.081	Plunging
13	0.49	2.40	0.09	0.10	4.281	14710	0.081	Plunging
14	0.51	2.82	0.12	0.15	7.796	41524	0.158	Plunging
15	0.45	2.00	0.13	0.15	5.315	27213	0.159	Plunging
16	0.46	2.04	0.08	0.09	3.224	9817	0.097	Plunging
17	0.45	2.00	0.08	0.09	2.959	8435	0.092	Plunging
18	0.45	1.80	0.08	0.09	2.655	7548	0.097	Plunging
19	0.45	1.83	0.10	0.12	3.560	13344	0.098	Plunging
20	0.46	2.21	0.10	0.11	4.854	20545	0.115	Plunging
21	0.46	2.20	0.12	0.15	5.387	25419	0.137	Plunging
22	0.48	2.23	0.11	0.15	4.901	20750	0.129	Plunging
23	0.51	2.20	0.15	0.21	6.438	36298	0.173	Plunging
24	0.51	2.40	0.14	0.16	7.051	39908	0.167	Plunging
25	0.50	2.40	0.14	0.17	7.235	42025	0.171	Plunging

2.6. Test procedure

At the beginning of each experiment, the ground level in the sediment reservoir was flattened and the wave maker started to generate the specified waves. The data in wave gauges no. 1 and 2 were recorded and wave reflection effects were removed as mentioned in section 2.3. The wave height in the breaking point and its distance to the pile were estimated from the recorded data in gauge no. 3 and horizontal and vertical photos of the wave breaking process as shown in Figs. 11 and 12. The experiments were continued until the equilibrium stage (equilibrium scour depth) was reached, as noted by Sumer and Fredsøe [2]. Then by digital camera, the necessary digital photos of the sediment reservoir bed were prepared from the locations mentioned in section 2.3. ArcGIS software was used for generation of DEM maps (Fig. 13). Then, they were revised and 3D maps were created by this software (Fig. 14). The detailed information is presented by Kiasalary and Mostafa Gharabaghi [34].

Figure 11. Typical horizontal photos from wave breaking process

Figure 12. A typical vertical photo from wave breaking process

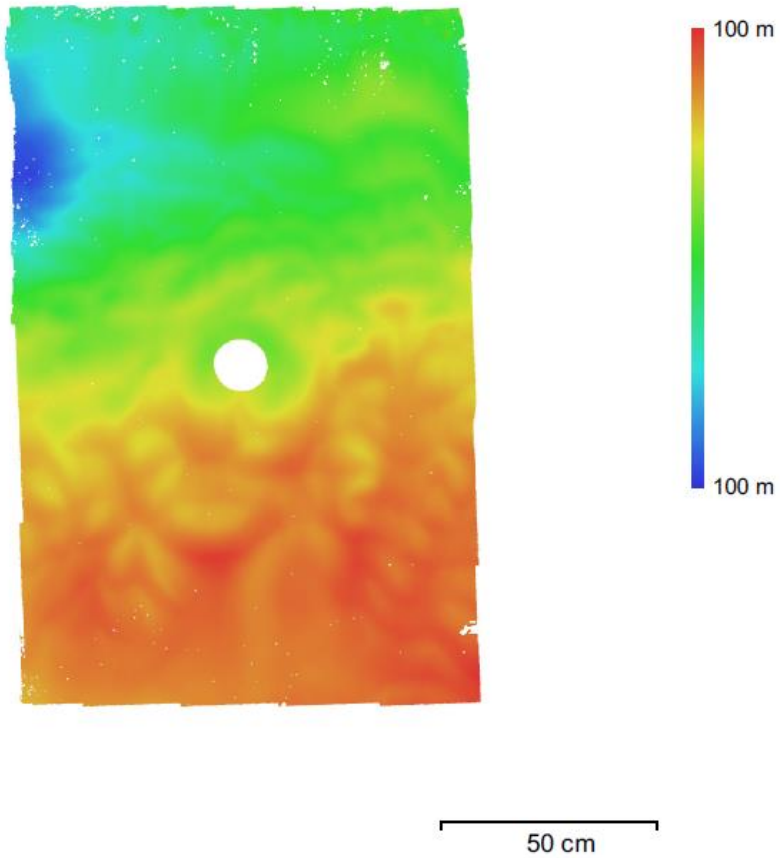

Figure 13. A typical reconstructed digital elevation model.

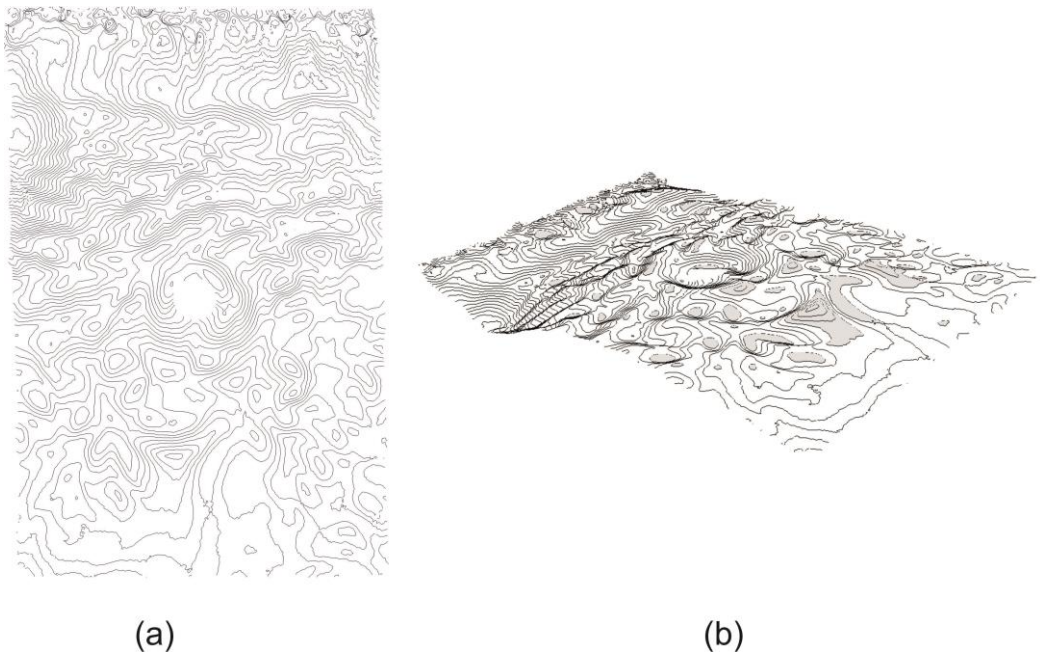

Figure 14. Typical a) 2D and b) 3D topographic map with counter lines.

3.Results and Discussion

Using AutoCAD software, the longitudinal profile and the dimensions of the bed form were determined. Based on the topographic maps, related photos and longitudinal profiles of experiments, two basic category of bed forms were identified. The first category is vortex ripples which is related to the experimental cases with KC < 6 and θ< 0.09, e.g., tests no. 1 and 2 as shown in Fig. 15. It can be deduced that the ripples are irregular 3 dimensional. The second category is truncated cone scour with vortex ripples, e.g., tests no. 17 and 18 as shown in Fig. 16. It can be deduced that the cones are truncated both in the plan and vertical direction

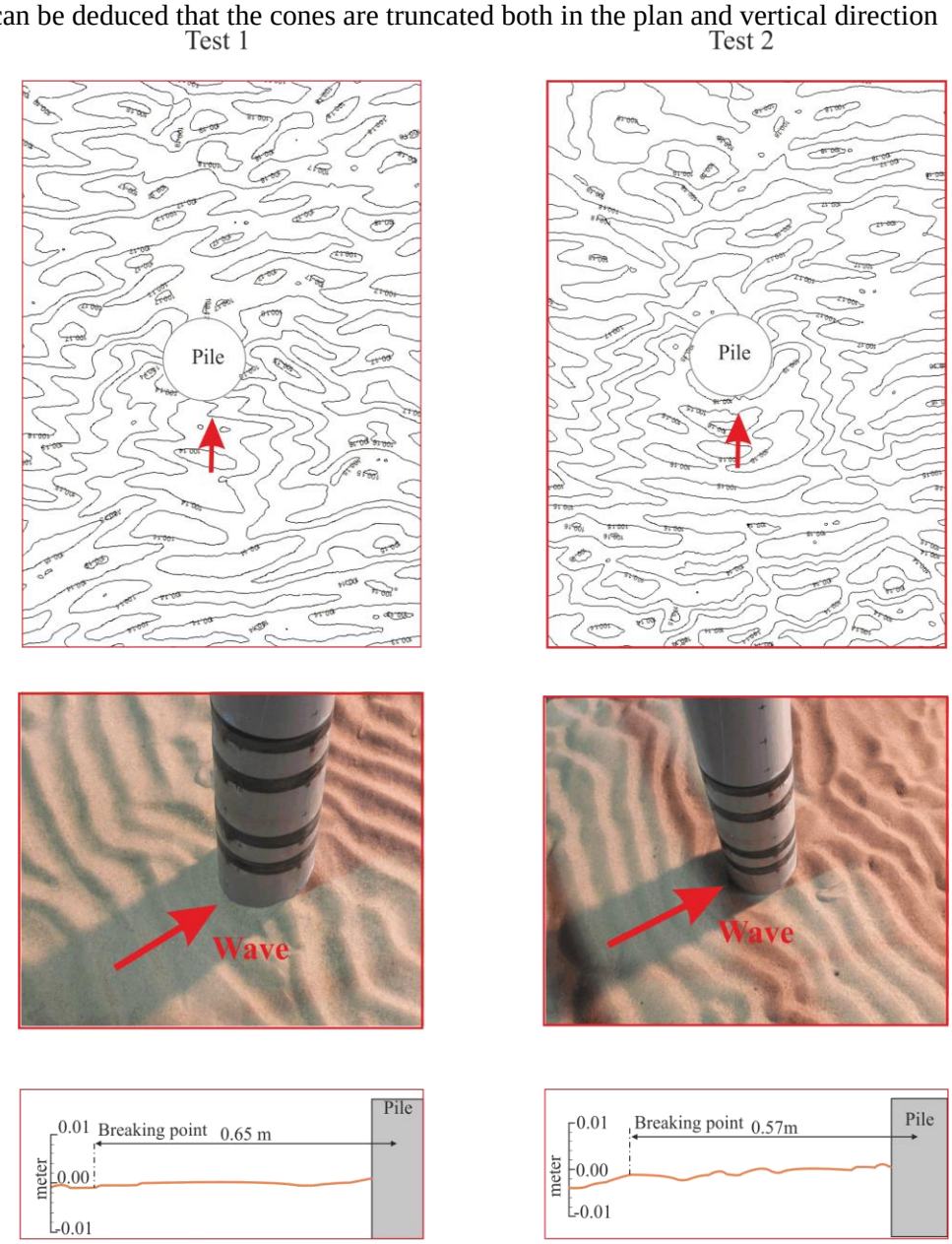

III-1.Vortex ripples

Figure 15. Photogrammetric maps, photos and longitudinal profiles of tests no. 1 and 2.

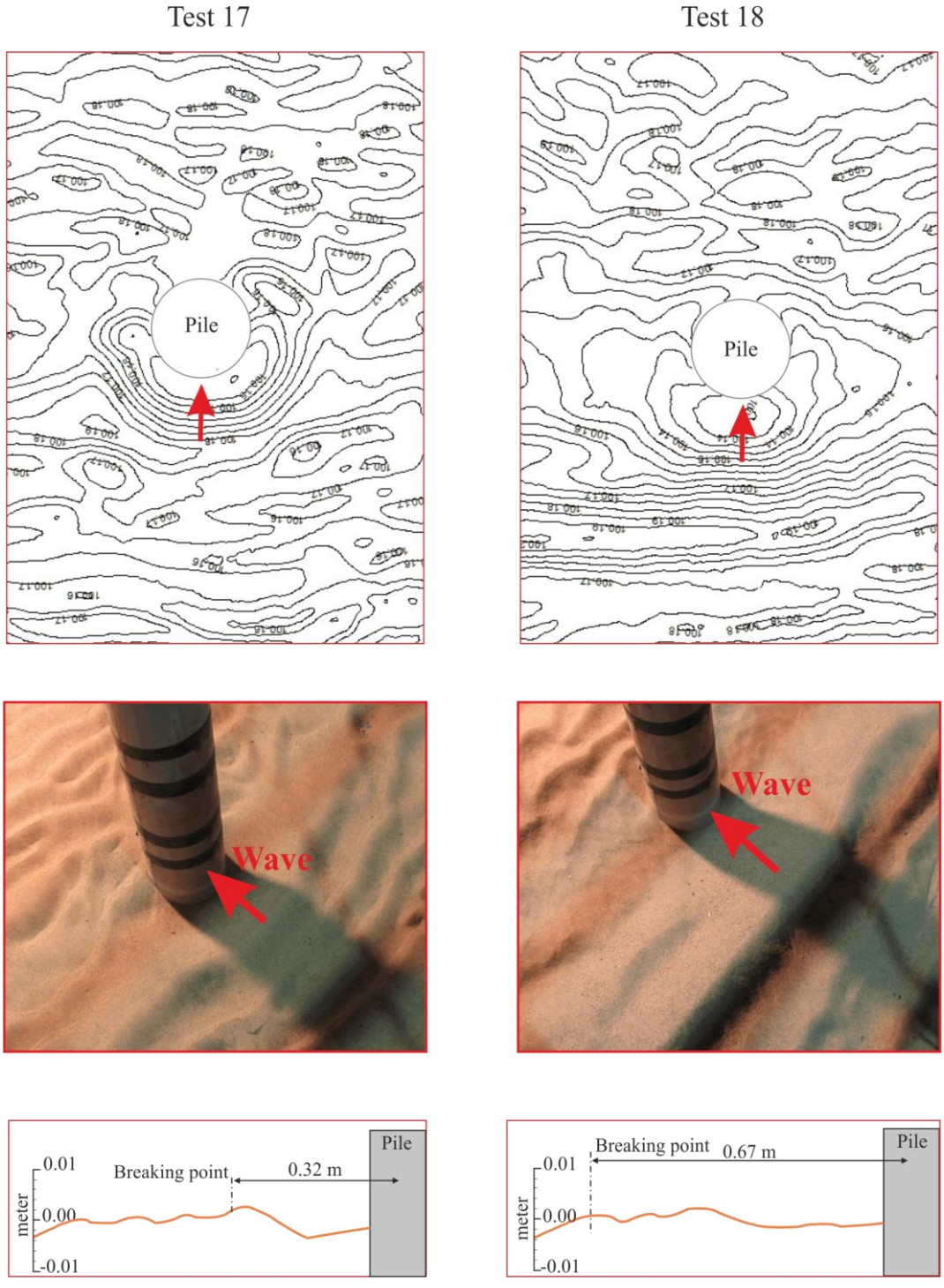

III-2.**Truncated cone scour with vortex ripples**

Figure 16. Photogrammetric maps, photos and longitudinal profiles of tests no. 17 and 18.

Concerning the bed form classification presented by Umeda [26] for non-breaking waves around the single pile (Fig. 2), it can be noticed that according to the present study, it should be revised for broken waves as presented in Fig. 17. The new classification has restricted the conditions for generation of vortex ripples to KC < 6 and θ < 0.09. It was mentioned in the introduction that for KC > 1, flow separation occurs leading to the formation of tail vortices and for KC > 6, horseshoe vortices are generated. Though it is acceptable that for KC < 6, vortex ripples are generated due to tail vortices. Moreover, according to the criterion given by Van Rijn [35], the critical value of θ_{crs} for initiation of sediment suspension is about 0.06 to 0.10 for the performed experiments. So, when the value of θ is larger than about 0.09, the sediment suspension starts before wave breaking and it is intensified after wave breaking leading to the bed form of truncated cone scour with vortex ripples, even for KC < 6.

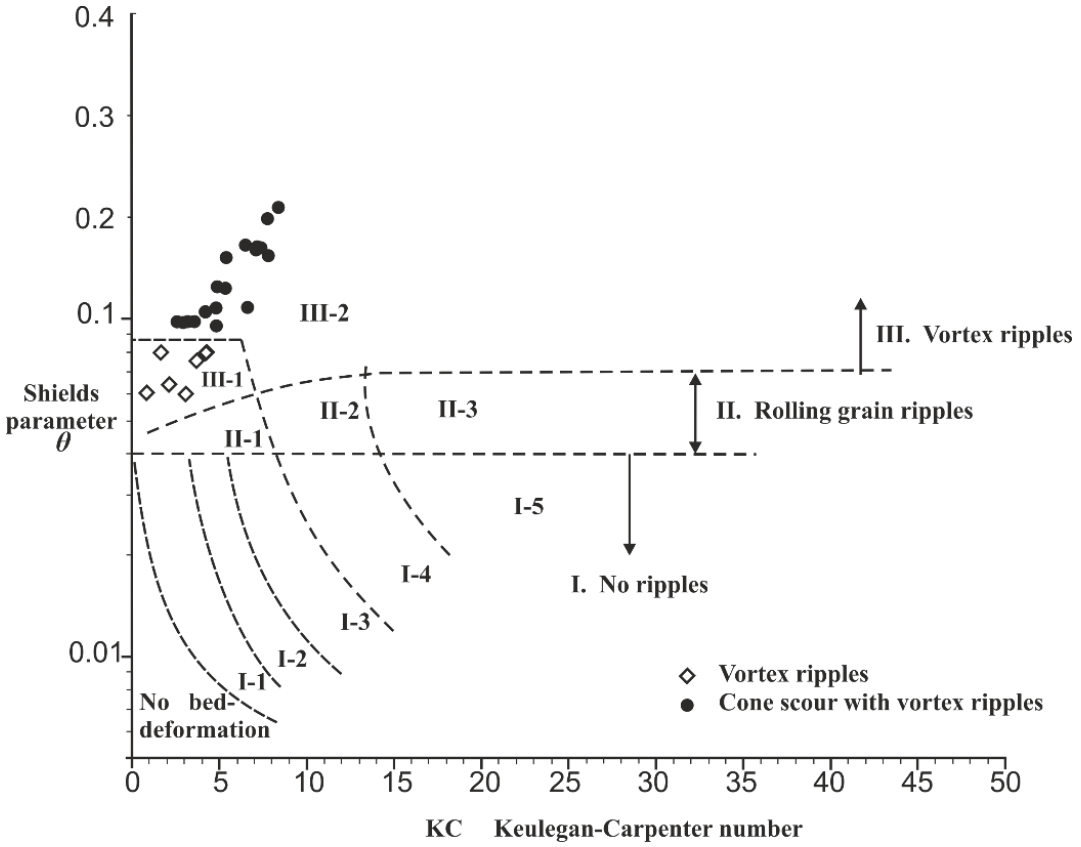

Figure 17. Modified Umeda's classification of bed form regimes for a vertical pile exposed to broken waves

In addition, it can be noticed that the ripple height and steepness for broken regular waves is less than non-breaking regular waves as part of wave energy is dissipated due to the wave breaking. In Fig. 18, the VFI (Vertical Form Index) of the ripples generated by broken waves which is the ratio of ripple length to its height, are compared with the values given by Allen [7] for non-breaking waves.

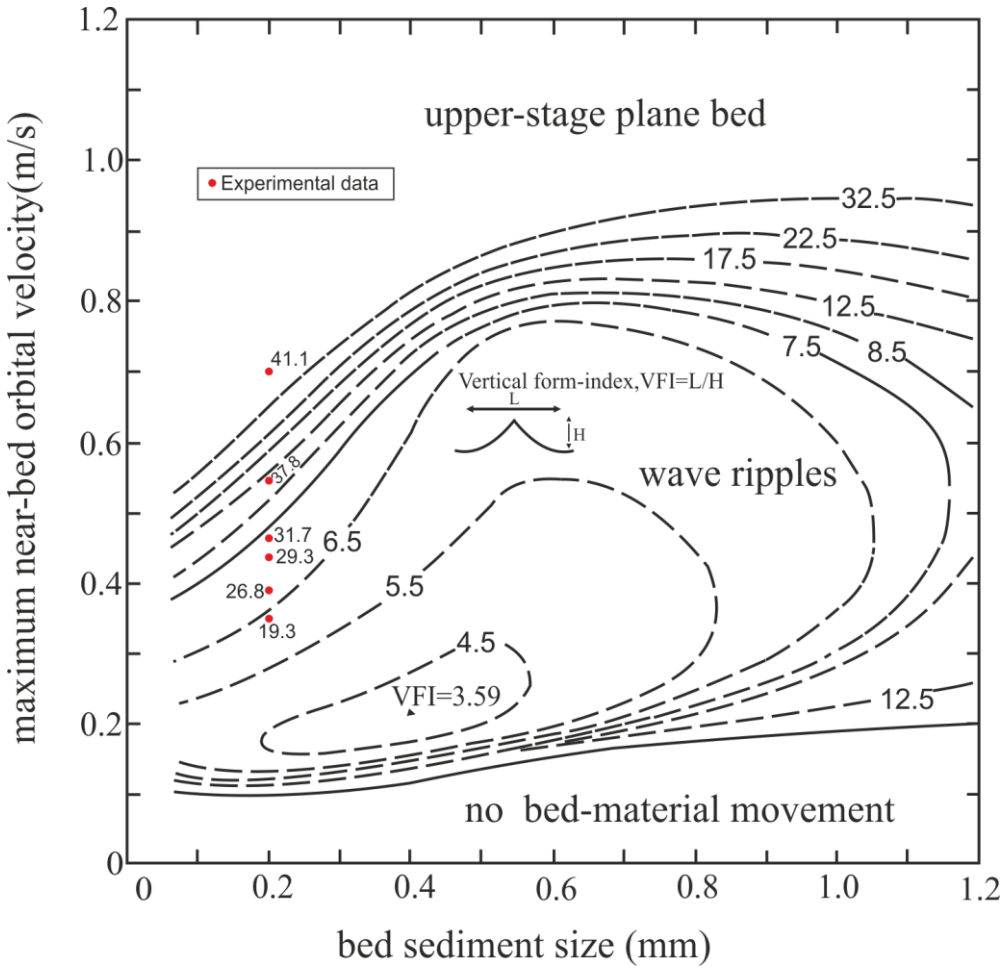

Figure 18. VFI (Vertical Form-Index) values of the ripples observed in the present study compared with values given by Allen [7]

In literature, there are several equations about the relative equilibrium scour depth (S/D, where S is the equilibrium scour depth) around vertical slender piles. According to Sumer et al. [12], for slender piles, it can be calculated by S/D = 1.3 (1 – exp (-0.03 (KC -6))), for KC > 6 as it assumes that horseshoe vortices are generated as KC gets larger than 6. However, it is observed in some cases with KC less than 6 [36]. Later, Dogan [36] modified their relation to S/D = 1.3 (1 – exp (-0.022 (KC-4))), for KC ≥ 4. In addition, Dogan [36] also obtained another equation for both slender and large piles by adding the D/L ratio (where L is the wave length) as the diffraction parameter, which reads: $S/D = 0.0037\ KC^{2/3} / (D/L)^{0.5}$. This equation didn't have the limitations given by the previous relations. In table 3, the results obtained from the present experiments are compared with the values given by these equations. It seems that the relative equilibrium scour depths for broken waves are larger than non-breaking waves.

Table 3. Comparison of the relative equilibrium scour depth obtained for broken waves in the present study with the values predicted for non-breaking waves

Test number	h(m)	T(sec)	H(m)	S/D Experimental measurement	S/D (Sumer et al. [12])	S/D (Modified eq. by Dogan [36])	S/D (New eq. of Dogan [36])
3	0.49	2.00	0.11	0.45	-	0.005	0.06
4	0.45	2.54	0.13	0.24	0.09	0.12	0.10
5	0.45	2.52	0.12	0.36	0.05	0.09	0.11
7	0.46	2.48	0.13	0.45	0.07	0.11	0.10
14	0.51	2.82	0.12	0.38	0.07	0.11	0.11
15	0.45	2.00	0.13	0.18	-	0.04	0.07
17	0.45	2.00	0.08	0.27	-	-	0.05
18	0.45	1.80	0.08	0.27	-	-	0.04
19	0.45	1.83	0.10	0.32	-	-	0.05
23	0.51	2.20	0.15	0.14	0.02	0.07	0.08

According to Fig. 19, based on the current experimental results the modified relation is developed for estimation of the relative equilibrium scour depth under broken waves:

$$\frac{S}{D} = 0.27\,E\exp(0.009KC)$$

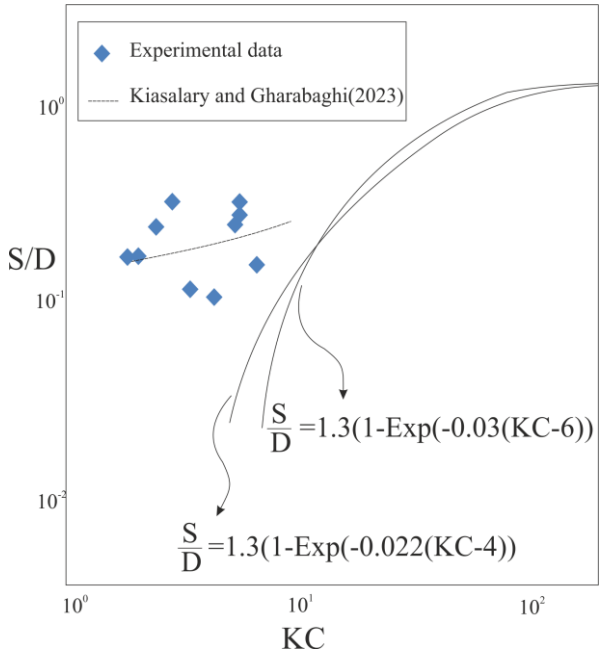

Figure 19. The relative equilibrium scour depth under broken waves versus KC number

It is obvious that as in the breaking zone, wave energy dissipation together with production of turbulent vortices occurs, so in spit that the wave energy is reduced so that the generated vortex ripples are flattened compared to the non-breaking waves, but as the wave breaking generated vortices impact to the vertical pile, the horseshoe vortices are generated even for smaller values of KC so that they can strongly erode the bed and generate deeper scours.

4. Conclusion

In this paper, the characteristics of bed forms around a vertical cylindrical pile due to the broken waves has been studied experimentally in a large wave flume. Close Range Photogrammetry was applied in order to measure the three-dimensional bed topography. 2-D and 3-D vortex ripples and truncated cone scour with vortex ripples were the main observed scour pattern.

The observed ripples have a sinusoidal shape and almost symmetrical with rounded profile. It is noticed that the ripple height and its steepness for broken regular waves is less than non-breaking regular waves. This is due to that some part of wave energy is dissipated after wave breaking.

However, for the truncated cone scours, the relative equilibrium scour depth (S/D) for broken waves is larger than non-breaking waves. This is also due to that, after wave breaking, plenty of turbulent vortices are produced; so highly aerated and turbulent bores impact to the pile, which can intensify the horseshoe vortices that can erode the bed deeply around the pile.

Umeda [26] investigated the bed forms around a single pile due to the waves. He used Shields parameter as well as Keulegan-Carpenter (KC) number as the non-dimensional parameters for bed form classification. It is noticed that according to the present study, it should be revised for broken waves as presented in Fig. 17.

5. Acknowledgment

This study was supported by the SCWMRI, Iran within the research project "Experimental study of breaking waves' effect on scouring depth and erosion pattern around single cylindrical piles in shallow water".

References

1. Sumer B.M., Christiansen N. and Fredsøe J., (1997). The horseshoe vortex and vortex shedding around a vertical wall-mounted cylinder exposed to waves. J. Fluid Mechanics, pp: 332:41-70.
2. Sumer B.M., Fredsøe L., The Mechanics of Scour in the Marine Environment, World Scientific Pub., Singapore, 2002.
3. Shields A., (1936). Anwendung der Ähnlichkeitsmechnik und der Turbulenz Forschung auf die Geschiebebewegung Mitt, der Preuss. Versuchsamst. Für Wasserbau und Schiffbau, Heft 26, Berlin, Deuschland.
4. Jonsson I.G., (1966). Wave boundary layer and friction factors. Proc. 10thCoastal Engineering Conf., Tokyo, Japan, pp: 1:127-148
5. Jonsson I.G., (1980). A new approach to oscillatory rough turbulent boundary layers. Ocean Engineering, pp: 7:109-152.
6. Fredsøe J., and Deigaard R., Mechanics of Coastal Sediment Transport. World Scientific Pub., Singapore, (1992).

7. Allen J.R.L., Sedimentary Structures, Their Character and Physical Basis. Elsevier's Science Pub., The Netherlands, (1982).
8. Dingler J.R., and Inman B.L., (1976). Wave-formed ripples in nearshore sands. Proc. 15th Coastal Engineering Conf., Honolulu, Hawaii, pp:
9. Horikawa K., Watanabe A., and Katori S., (1982). Sediment transport under sheet flow conditions. Proc. 18thCoastal Engineering Conf., Cape Town, S. Africa, pp: II: 1335-1352
10. Wilson K.C., (1989). Friction of wave-induced sheet flow. Coastal Engineering, pp: 12.
11. Chiew Y.M. and Melville B.W., (1987). Local scour around bridge piers. J. Hydraulic research, pp: 25(1):15-26.
12. Sumer B. M., Fredsøe J., and Christiansen N., (1992). Scour around vertical pile in waves. Journal of waterway, port, coastal, and ocean engineering, pp: 118(1):15-31.
13. Melville B.W., (1997). Pier and abutment scour: integrated approach. Journal of hydraulic Engineering, pp: 123(2):125-136.
14. Melville B. and Coleman S., Bridge scour, Water Resources Pub., LLC, Colorado, 2000.
15. Sumer B. M., Whitehouse R. J., and Tørum A., (2001). Scour around coastal structures: a summary of recent research. Coastal Engineering, pp: 44(2):153-190.
16. Sumer B.M., Fredsøe L., (2001). Wave scour around a large vertical circular cylinder. Journal of waterway, port, coastal, and ocean engineering, pp: 127(3):20520.
17. Sheppard, D. M. Large-scale and live-bed local pier scour experiments. Coastal Engineering Technical Rep. No. 133, Civil and Coastal Engineering Dept., Univ. of Florida, Gainesville, 2003.
18. Coleman S., (2005). Clear water local scour at complex piers. J. Hydraul. Eng., pp: 131(4): 330–334.
19. Elsebaie I.H., (2013). An experimental study of local scour around circular bridge pier in sand soil. International Journal of Civil & Environmental Engineering IJCEE-IJENS, pp: 13(01):23-28, 2013.
20. Amini Baghbadorani D., Beheshti A.A., and Ataie-Ashtiani B., (2017). Scour hole depth prediction around pile groups: review, comparison of existing methods, and proposition of a new approach. Natural Hazards, pp: 88:977-1001.
21. Chen B., and Li S. (2018). Experimental study of local scour around a vertical cylinder under wave only and combined wave-current conditions in a large-scale flume. J. of Hydraulic Engineering, pp:144(9):04018058.
22. Gazi A.H., Afzal M. S., and Dey S., (2019). Scour around piers under waves: Current status of research and its future prospect. Water, pp: 11:2212.
23. Liang B., Du S., Pan X., and Zhang L., (2019). Local scour for vertical piles in steady currents: review of mechanisms, influencing factors and empirical equations. Journal of Marine Science and Engineering, pp: 8(1):4.
24. Guan D., Xie Y., Yao Z., Chiew Y., Zhang L. and Zheng J., (2022). Local scour at offshore wind farm mono pile foundations: A review. Water Science and Engineering, pp:15(1):29-39.

25. Li J., Guo Y., Lian J., and Wang H., (2023). Mechanisms, assessments, countermeasures, and prospects for offshore wind turbine foundation scour research. Ocean Engineering, pp: 281 (114893).
26. Umeda S., (2011). Scour regime and scour depth around a pile in waves. J. of Coastal Research, pp: 64:845-849.
27. Otsuka J., Saruwatari A., and Watanabe Y., (2017). Vortex-induced suspension of sediment in the surf zone. Advances in Water Resources, pp: 110: 59-76.
28. Bijker E.W., and de Bruyn C.A., (1988). Erosion around the pile due to the current and breaking waves. Proc. 21st. Coastal Engineering Conf., ASCE, Reston, USA, pp: 2:1368-1381.
29. Carreiras J., Larroudé Ph., Seabra-Santos F.J., and Mory M., (2000). Wave scour around piles. Proc. 27th Coastal Engineering Conf., ASCE, Sydney, Australia, pp: 2:1860-1870.
30. Frigaard P., Hansen E.A., Christensen E.D. and Jensen M.S., (2005). Effect of breaking waves on scour processes around circular offshore wind turbine foundations. NWTC External Web Site National Wind Technology Center.
31. Nielsen A.W., Sumer B.M., Ebbe S.S., and Fredsøe J. (2012). Experimental study on the scour around a monopile in breaking waves. Journal of waterway, port, coastal, and ocean engineering, pp:138(6):501-506.
32. LiuX., Liu C., Zhu X., He Y., Wang Q. and Wu Z., (2020). 3D modeling and mechanism analysis of breaking wave-induced seabed scour around monopile. Mathematical Problems in Engineering. https://doi.org/10.1155/2020/1647640.
33. Goda Y., and Suzuki T., (1976). Estimation of incident and reflected waves in random wave experiments. Proc. 15th International Conference on Coastal Engineering., ASCE, Honolulu, USA, pp:828-845.
34. Kiasalary A., and Mostafa Gharabaghi A.R., (2023). Estimation of Bed Topography near the Cylindrical Pile under Breaking Waves by Close Range Photogrammetry. Int. J. of Coastal, Offshore and Environmetal Engineering, pp: 8(3): 32-39.
35. Van Rijn L.C., Handbook of sediment transport by currents and waves. Report H461, Delft Hydraulics, Delft, Netherlands, 1989.
36. Dogan M., (2021). The equilibrium depth of wave scours around both slender and large piles. Ocean Engineering, pp: 236: 109474.